



OPEN

Mixed lanthanide oxide nanoparticles as dual imaging agent in biomedicine

SUBJECT AREAS:
IMAGING TECHNIQUES
AND AGENTS
NANOPARTICLESWenlong Xu¹, Badrul Alam Bony¹, Cho Rong Kim¹, Jong Su Baek², Yongmin Chang², Ji Eun Bae³, Kwon Seok Chae⁴, Tae Jeong Kim⁵ & Gang Ho Lee¹

¹Department of Chemistry, College of Natural Sciences, Kyungpook National University (KNU), Taegu 702-701, South Korea, ²Department of Molecular Medicine and Medical & Biological Engineering, School of Medicine, KNU and Hospital, Taegu 702-701, South Korea, ³Department of Nanoscience and Nanotechnology, KNU, Taegu 702-701, South Korea, ⁴Department of Biology Education, Teachers' College, KNU, Taegu 702-701, South Korea, ⁵Department of Applied Chemistry, College of Engineering, KNU, Taegu 702-701, South Korea.

Received
2 September 2013Accepted
29 October 2013Published
13 November 2013

Correspondence and requests for materials should be addressed to Y.M.C. (ychang@knu.ac.kr); K.S.C. (kschae@knu.ac.kr) or G.H.L. (ghlee@mail.knu.ac.kr)

There is no doubt that the molecular imaging is an extremely important technique in diagnosing diseases. Dual imaging is emerging as a step forward in molecular imaging technique because it can provide us with more information useful for diagnosing diseases than single imaging. Therefore, diverse dual imaging modalities should be developed. Molecular imaging generally relies on imaging agents. Mixed lanthanide oxide nanoparticles could be valuable materials for dual magnetic resonance imaging (MRI)-fluorescent imaging (FI) because they have both excellent and diverse magnetic and fluorescent properties useful for dual MRI-FI, depending on lanthanide ions used. Since they are mixed nanoparticles, they are compact, robust, and stable, which is extremely useful for biomedical applications. They can be also easily synthesized with facile composition control. In this study, we explored three systems of ultrasmall mixed lanthanide (Dy/Eu, Ho/Eu, and Ho/Tb) oxide nanoparticles to demonstrate their usefulness as dual T₂ MRI-FI agents.

There is a continuing research interest in mixed lanthanide oxide nanoparticles because they have both magnetic and fluorescent properties useful for dual imaging in biomedicine¹⁻¹⁰. By using different lanthanide ions in synthesis, a variety of mixed lanthanide oxide nanoparticles can be synthesized. These mixed nanoparticles generally have an advantage over core-shell¹¹, hetero-junction¹², and dye-coated nanoparticles¹³ because of their compactness, robustness, stability, and easy synthesis with composition control. In addition, several inherent magnetic and fluorescent properties of mixed lanthanide oxide nanoparticles are valuable in molecular imaging. First, their magnetic and fluorescent properties are not much affected by surface coating due to compactness of 4f-orbitals close to nucleus¹⁴. Second, their magnetic properties do not change much with particle diameter for the same reason¹⁴. Third, their fluorescent intensities enhance with decreasing particle diameter due to reduced excitation migration to quenching sites that are proportional to particle diameter^{15,16}. Therefore, ultrasmall mixed lanthanide oxide nanoparticles will be extremely useful for dual magnetic resonance imaging (MRI)-fluorescent imaging (FI), as demonstrated in this study.

There is no doubt that dual imaging will play a vital role in diagnosing diseases in the near future. First, dual imaging can generally provide more information useful for diagnosing diseases than the single imaging does^{17,18}. Injection doses can be reduced because a single dose of a dual imaging agent will cover both doses of single imaging agents. Regarding MRI-FI, MRI generally has a high spatial resolution of ~ 1 mm while FI, a very high sensitivity that is limited by that of an optical device^{19,20}. Therefore, a dual MRI-FI modality will allow us to detect and diagnose diseases very sensitively and in a high spatial resolution²¹.

This study deals with T₂ MRI-FI agents. While FI entirely relies on chemical agents, MRI is greatly improved using contrast agents through contrast enhancements. Here, it is worth to mention that a good MRI contrast agent should satisfy that it should be non-toxic, completely excreted from a body through renal system after some time after intravenous injection, should have a large r₁ value and r₂/r₁ ratio close to one in case of a T₁ MRI contrast agent, and a large r₂ value in case of a T₂ MRI contrast agent to show high contrast MR images at a standard injection dose. T₂ MRI contrast agents can be made by nanoparticles but not by molecules because large magnetic moments at room temperature are needed in accelerating transverse water proton relaxation that is induced by fluctuation of local magnetic field generated by nanoparticles²²⁻²⁴. Although lanthanide oxide nanoparticles have only decent magnetic moments at room temperature, they are useful at high MR fields^{25,26}. Their magnetic moments are decent even at ultrasmall particle diameters, extremely useful for in vivo applications



Table 1 | Basic magnetic and fluorescent properties of precursor lanthanide (Ln) ions used in this study

Ln ³⁺	Ground state configuration	Fluorescent color	Theoretical magnetic moment (μ_B)	Observed magnetic moment (μ_B)	Applicable imaging	Ref.
Eu ³⁺	⁷ F ₀ (4f ₆)	Red	0	3.3–3.5	FI	14,28
Tb ³⁺	⁷ F ₆ (4f ₈)	Green	9.72	9.5–9.8	T ₂ MRI, FI	14,28
Dy ³⁺	⁶ H _{15/2} (4f ₉)	-	10.65	10.4–10.6	T ₂ MRI	14,28
Ho ³⁺	⁵ I ₈ (4f ₁₀)	-	10.6	10.4–10.7	T ₂ MRI	14,28

because only ultrasmall nanoparticles can be excreted through renal system²⁷. They can also have diverse fluorescent colours, depending on lanthanide elements^{14,28,29}. Their fluorescent properties are similar to quantum dots (QDs) except for their weaker fluorescent intensities. That is, they have narrow band widths useful for multiplex imaging and high photostabilities like QDs^{30,31}, which are superior to dyes because dyes have wide band widths³² and poor photostabilities (i.e., subject to photobleaching and photodecomposition after multiple uses)²⁸. Lower fluorescent intensities of lanthanide oxide nanoparticles than those of QDs and dyes can be partly overcome through the imaging depth increase using up-conversion compositions^{33–35}.

As summarized in Table 1, Dy, Ho, and Tb have large magnetic moments¹⁴ while Eu and Tb strongly fluoresce in visible region^{14,28,29}. Although not listed in Table 1, Gd and Er also have large magnetic moments comparable to those of the above three elements¹⁴. Therefore, ultrasmall mixed lanthanide oxide nanoparticles composed of these elements will be useful for both MRI and FI. Their basic applications to biomedical imagings are schematically represented in Fig. 1. In this study, we explored three systems of ultrasmall mixed lanthanide (Dy/Eu, Ho/Eu, and Ho/Tb) oxide nanoparticles to demonstrate their usefulness as T₂ MRI-FI agents by investigating their *in vivo* T₂ MR images and *in vitro* fluorescent confocal images.

Results

Composition, particle diameter, and hydrodynamic diameter.

Compositions in Dy_xEu_yO₃, Ho_xEu_yO₃, and Ho_xTb_yO₃ nanoparticles were estimated to be (x, y) = (1.5 ± 0.1, 0.5 ± 0.1), (1.6 ± 0.1, 0.4 ± 0.1), and (1.1 ± 0.1, 0.9 ± 0.1), respectively, using an inductively coupled plasma atomic emission spectrometer (ICPAES). x and y values were similar to precursor ion molar ratios used in synthesis within an experimental error limit, implying that reaction properties of all lanthanide ions are similar to one another likely due to their identical trivalent ionic state and similar ionic radii. Therefore, composition can be easily controlled just by varying precursor ion molar ratios.

Particle diameters were estimated using two electron microscopes (EMs) with different acceleration voltages. D-glucuronic acid coated nanoparticles are hydrophilic because they are coated with hydrophilic D-glucuronic acids and thus were not monodispersed but mostly aggregated in EM images because they were dispersed on hydrophobic carbon film on copper grid. This is opposite to hydrophobic nanoparticles synthesized in organic solvents that can be monodispersed on carbon film^{36,37}. From high resolution transmission electron microscope (HRTEM) and high voltage electron microscope (HVEM) images in Fig. 2A, the average core particle diameters (d_{avg}) of D-glucuronic acid coated ultrasmall Dy_{1.5}Eu_{0.5}O₃, Ho_{1.6}Eu_{0.4}O₃, and Ho_{1.1}Tb_{0.9}O₃ nanoparticles were estimated to be 2.3 ± 0.1, 2.1 ± 0.1, and 2.5 ± 0.1 nm, respectively, using log-normal function fits to observed particle diameter distributions as shown in Fig. 2B. HVEM images are also provided for Ho_{1.1}Tb_{0.9}O₃ nanoparticles with an improved lattice resolution. More HRTEM and HVEM images are provided in Supplementary data.

Low resolution TEM and elemental map images are shown in Fig. 2C. Since nanoparticles are so ultrasmall that an elemental map image of each individual nanoparticle could not be obtained. Therefore, we provided overall elemental map images of nanoparticles. As expected, identical elemental map images for all elements in each sample were observed, implying that nanoparticles are mixed (or alloy) Ln^a_xLn^b_yO₃ nanoparticles but not physical mixtures of Ln^a₂O₃ and Ln^b₂O₃ nanoparticles. The doping-induced particle size tuning effect as observed in up-conversion NaYF₄:Yb/Er nanocrystals³⁸ may not be observed in the present mixed nanoparticles. This is because of similar ionic radii and similar reaction properties between lanthanide ions.

From dynamic light scattering (DLS) patterns in Fig. 2D, the average hydrodynamic diameters (a_{avg}) of D-glucuronic acid coated ultrasmall Dy_{1.5}Eu_{0.5}O₃, Ho_{1.6}Eu_{0.4}O₃, and Ho_{1.1}Tb_{0.9}O₃ nanoparticles were estimated to be 6.7 ± 0.1, 6.4 ± 0.1, and 7.6 ± 0.1 nm, respectively. Pictures of well-dispersed aqueous sample solutions are also inserted in Fig. 2D.

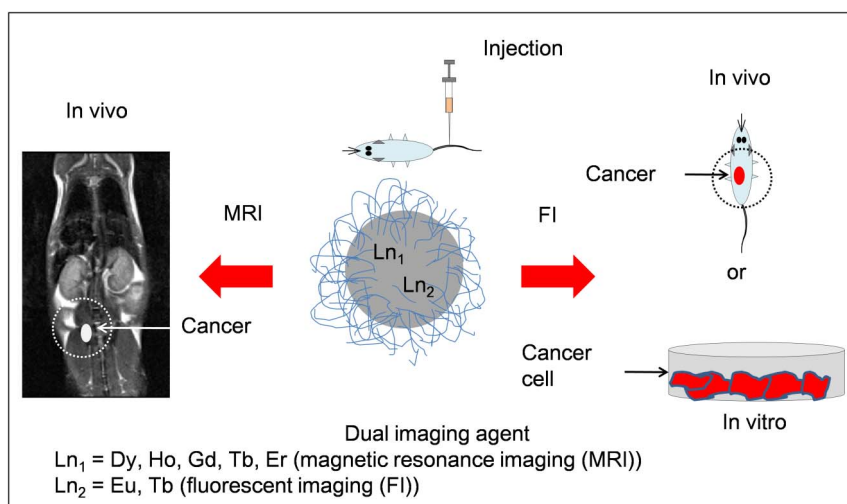


Figure 1 | A schematic diagram showing possible applications of ultrasmall mixed lanthanide oxide nanoparticles in the area of MRI and FI.

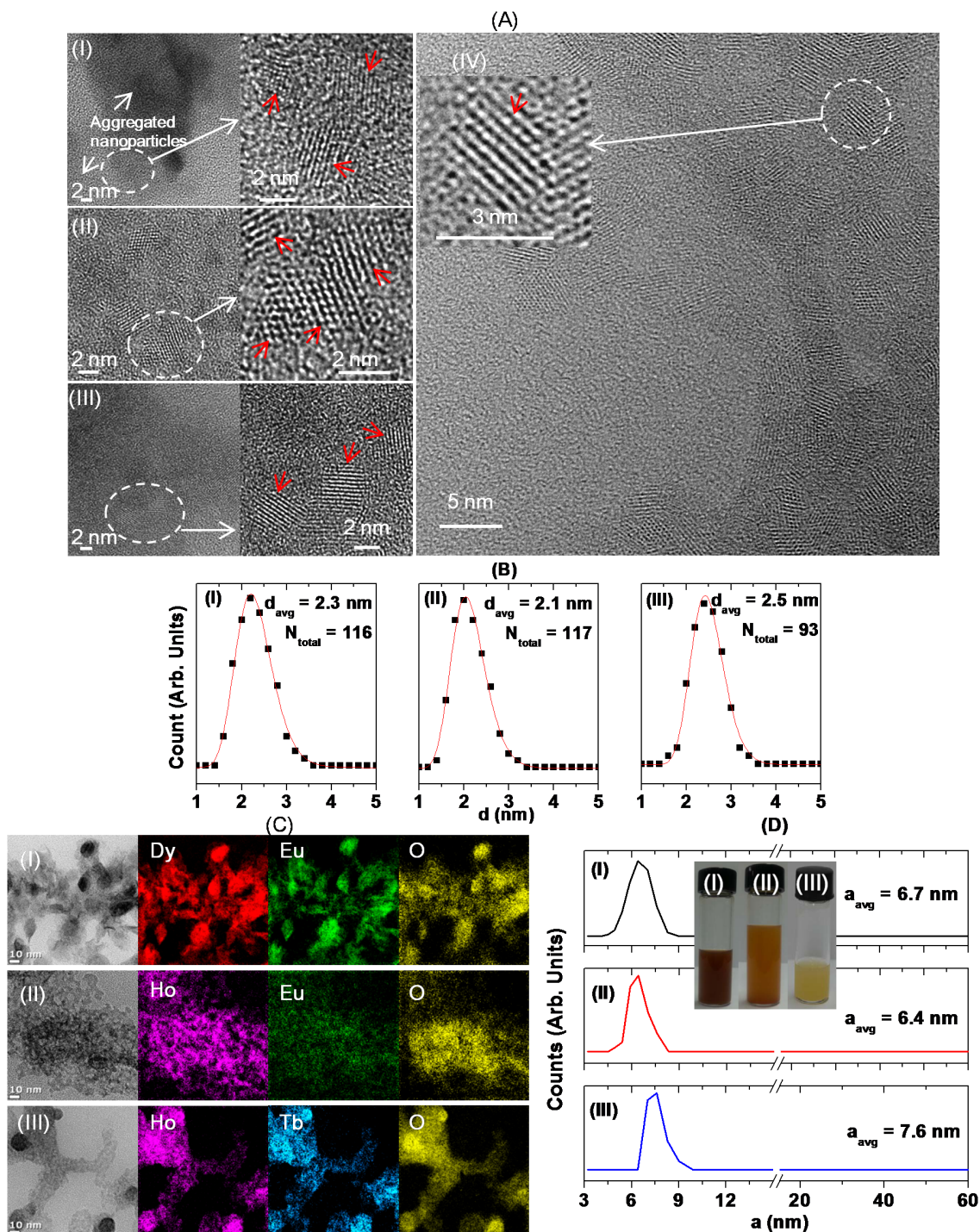


Figure 2 | (A) HRTEM and HVEM images. Selected areas (i.e., dotted circles) in each HRTEM and HVEM image were magnified and nanoparticles in magnified images were indicated with arrows. (B) Log-normal function fits to observed particle diameter distributions (N_{total} indicates the total number of nanoparticles used in the fit and d_{avg} , the average particle diameter estimated from the fit). (C) Low resolution TEM and elemental map images at 10 nm scale. (D) DLS patterns of aqueous sample solutions and photographs of the corresponding aqueous sample solutions. Common from (A) to (D), (I) indicates D-glucuronic acid coated ultrasmall $Dy_{1.5}Eu_{0.5}O_3$ nanoparticles, (II), D-glucuronic acid coated ultrasmall $Ho_{1.6}Eu_{0.4}O_3$ nanoparticles, and (III) and (IV), D-glucuronic acid coated ultrasmall $Ho_{1.1}Tb_{0.9}O_3$ nanoparticles.

We also investigated crystal structures of powder samples of D-glucuronic acid coated ultrasmall mixed lanthanide oxide nanoparticles by measuring X-ray diffraction (XRD) patterns (Supplementary data). As-prepared powder samples showed very broad patterns as observed in unmixed nanoparticles³⁹ whereas powder samples after thermal treatment with a thermogravimetric analyzer (TGA) showed sharp peaks, all corresponding to a highly crystallized cubic Ln_2O_3 due to particle size growth during TGA treatment^{25,39}.

Surface coating. Nanoparticles should be coated with water-soluble and biocompatible ligands for biomedical applications. D-glucuronic acid was used in this study. The surface coating was investigated by recording Fourier transform-infrared (FT-IR) absorption spectra of powder samples of D-glucuronic acid coated ultrasmall mixed lanthanide oxide nanoparticles in pallet forms in KBr as shown in Fig. 3A. A FT-IR absorption spectrum of a free D-glucuronic acid was also recorded as a reference as shown in Fig. 3A. Stretching

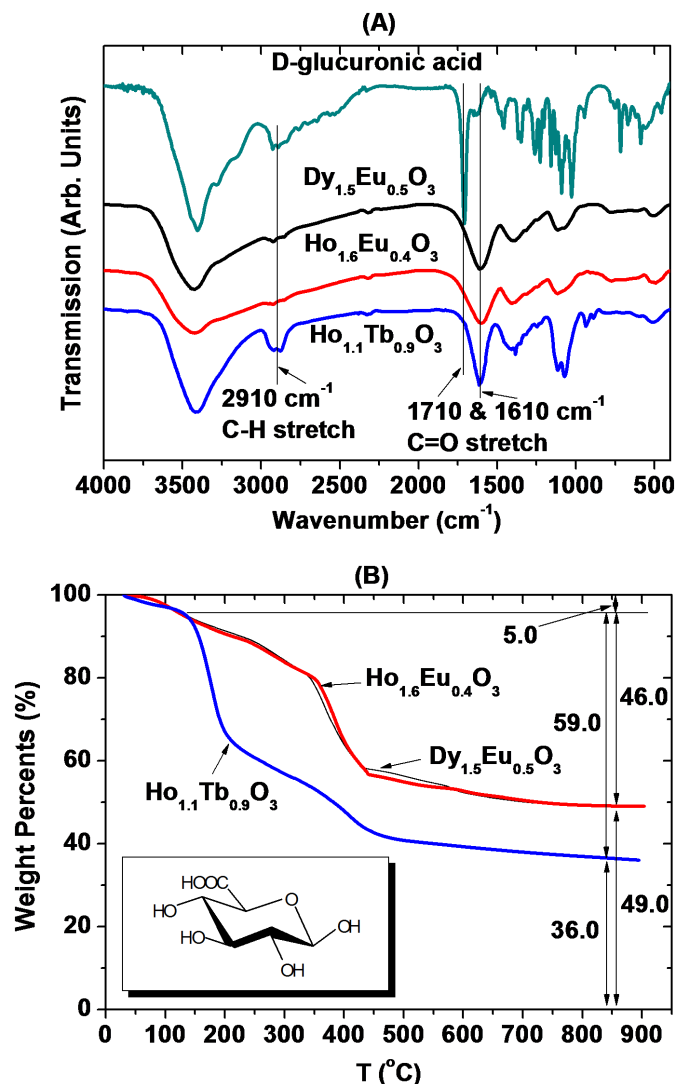


Figure 3 | (A) FT-IR absorption spectra of a free D-glucuronic acid and three powder samples of D-glucuronic acid coated ultrasmall mixed lanthanide oxide nanoparticles. (B) TGA curves of three powder samples of D-glucuronic acid coated ultrasmall mixed lanthanide oxide nanoparticles. Inserted in (B) at the left bottom is a molecular structure of D-glucuronic acid used for surface coating of nanoparticles.

frequencies characteristic of C–H at 2910 cm⁻¹, C=O at 1610 cm⁻¹, and C–O at 1070 cm⁻¹ of D-glucuronic acid in powder samples confirmed the surface coating. Furthermore, the C=O stretch was red-shifted by ~ 100 cm⁻¹ from that (= 1710 cm⁻¹) of a free D-glucuronic acid, confirming that its –COOH group was bonded to a nanoparticle. This red shift has been observed in various metal oxide nanoparticles coated with ligands with –COOH group^{39–43}, supporting our results. TGA curves were also recorded to estimate the amount of surface coating with D-glucuronic acid as shown in Fig. 3B. The surface coating weight percentages were estimated to be 46.0% for Dy_{1.5}Eu_{0.5}O₃, 46.0% for Ho_{1.6}Eu_{0.4}O₃, and 59.0% for Ho_{1.1}Tb_{0.9}O₃ nanoparticles from the mass drop in the corresponding TGA curves. 5.0% water desorption between room temperature and ~ 110°C was taken into account in all of these values. The remaining corresponded to net masses of ultrasmall Dy_{1.5}Eu_{0.5}O₃, Ho_{1.6}Eu_{0.4}O₃, and Ho_{1.1}Tb_{0.9}O₃ nanoparticles in powder samples. The surface coating weight percentages were converted into average grafting densities corresponding to the average number of D-glucuronic acids coated per unit surface area of a nanoparticle^{25,44}. They were estimated to be 9.4, 8.3, and 17.3 nm⁻² for D-glucuronic acid coated

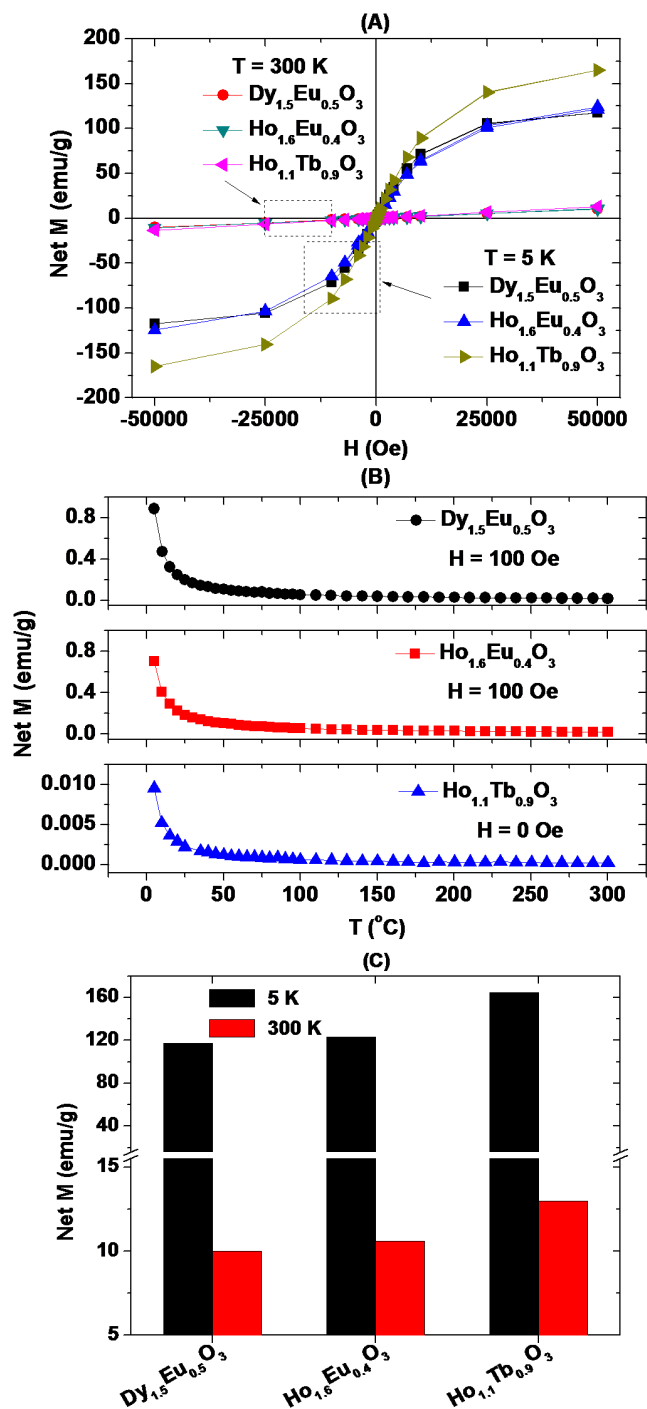


Figure 4 | (A) Mass-corrected M-H curves at T = 5 and 300 K and (B) mass-corrected ZFC M-T curves at H = 0 or 100 Oe of three powder samples of D-glucuronic acid coated ultrasmall mixed lanthanide oxide nanoparticles. (C) Histogram of net magnetizations estimated from M-H curves at H = 5 tesla and T = 5 and 300 K.

ultrasmall Dy_{1.5}Eu_{0.5}O₃, Ho_{1.6}Eu_{0.4}O₃, and Ho_{1.1}Tb_{0.9}O₃ nanoparticles, respectively. All of these values were larger than 1.0, showing sufficient surface coating of nanoparticles with D-glucuronic acid⁴⁴.

Magnetic properties. Magnetic properties of ultrasmall mixed lanthanide oxide nanoparticles were investigated by recording both magnetization (M) versus applied field (H) (i.e., M-H) curves (–5 ≤ H ≤ 5 tesla) at temperatures (T) = 5 and 300 K (Fig. 4A) and zero-field-cooled (ZFC) M-T curves (5 ≤ T ≤ 300 K) at H = 0 or 100



oersted (Oe) (Fig. 4B). Here, magnetizations in Fig. 4 corresponded to net magnetizations of ultrasmall mixed lanthanide oxide nanoparticles in powder samples because they were mass-corrected with net masses of nanoparticles in powder samples as described in experimental section. Both coercivities and remanences in M–H curves were zero (i.e., no hysteresis). This lack of hysteresis and no magnetic transition down to $T = 5$ K in all M–T curves showed that all ultrasmall mixed lanthanide oxide nanoparticles were paramagnetic down to 5 K, consistent with previous reports^{45–48}. Therefore, magnetizations in all samples arise from electron magnetic moments of Dy^{3+} (${}^6\text{H}_{15/2}$), Ho^{3+} (${}^5\text{I}_8$), and Tb^{3+} (${}^7\text{F}_6$) (see Table 1). Net magnetizations of ultrasmall mixed lanthanide oxide nanoparticles estimated from M–H curves at $T = 5$ and 300 K were plotted in Fig. 4C. As shown in Fig. 4C, net magnetizations at $T = 300$ K are decent due to unsaturated magnetizations at room temperature, whereas those at $T = 5$ K are large due to nearly saturated magnetizations. Magnetizations at room temperature are important for water proton relaxation because the water proton relaxivity (r) is

proportional to the square of magnetization^{22–24} and thus, should be as large as possible.

Relaxivities and map images. Both inverse longitudinal ($1/T_1$) and transverse ($1/T_2$) relaxation times measured at 1.5 tesla and 22°C were plotted as a function of Ln ($\text{Ln} = \text{Dy}$ or Ho) concentration in Fig. 5A and combined Ln₁&Ln₂ ($\text{Ln}_1 = \text{Dy}$ or Ho , $\text{Ln}_2 = \text{Eu}$ or Tb) concentration in Fig. 5B. Longitudinal (r_1) and transverse (r_2) water proton relaxivities were estimated from the corresponding slopes (i.e., from the equation $1/T_i = r_i C + I$ ($i = 1$ or 2) in which C is the concentration and I , the intercept) and plotted in Fig. 5C. As shown in Fig. 5C, r_1 values were negligible in all samples (i.e., less than $1.0 \text{ s}^{-1}\text{mM}^{-1}$) because of orbital contribution to magnetic moments in Dy^{3+} , Ho^{3+} , and Tb^{3+} . Note that only a pure electron spin magnetic moment as in Gd^{3+} can strongly induce a longitudinal water proton relaxation^{22,23}. In fact, gadolinium oxide and gadolinium-based nanoparticles have shown very large r_1 values^{49–52}. However, r_2 values, depending on total magnetic moment of contrast agents²⁴,

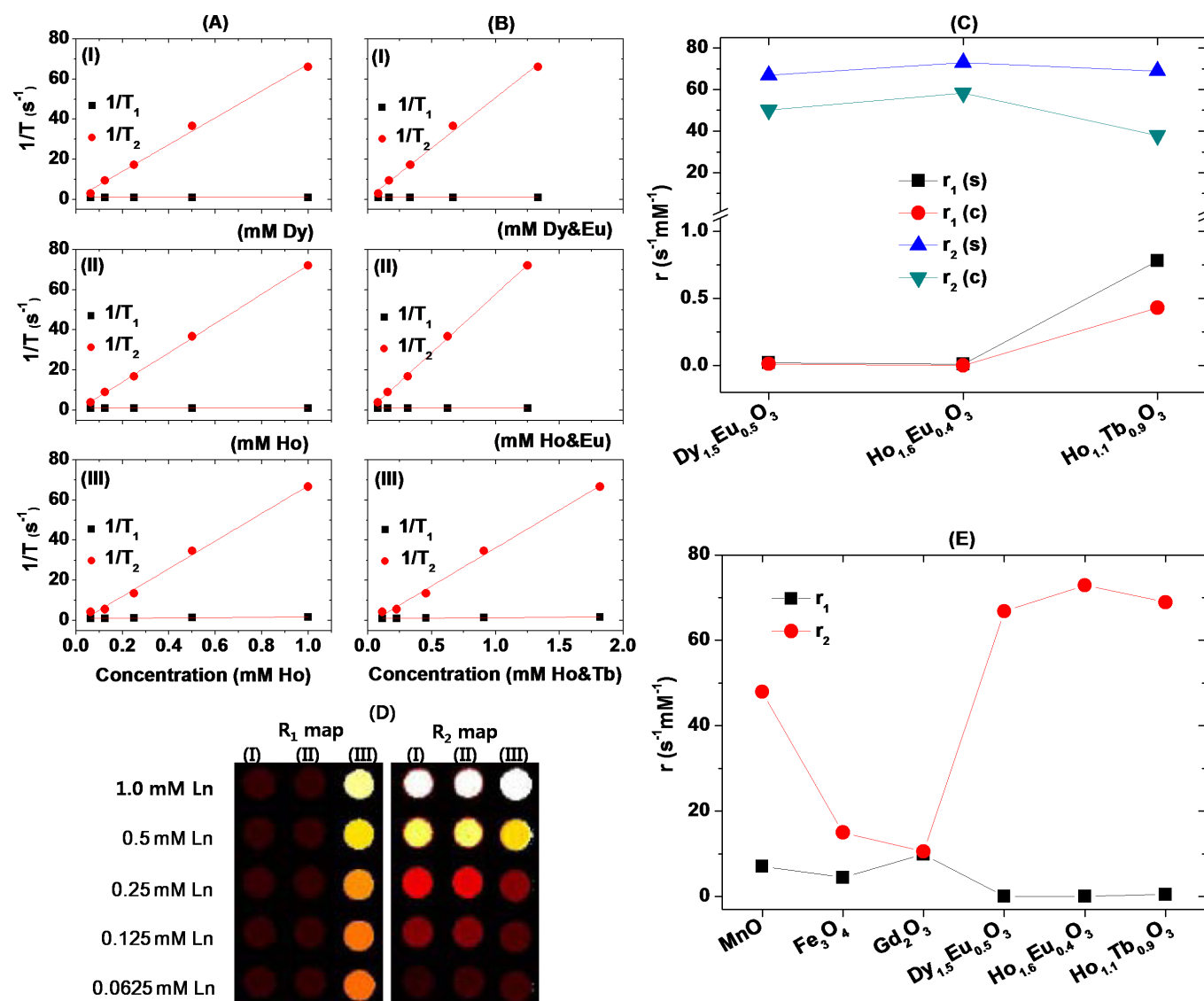


Figure 5 | Plots of $1/T_1$ and $1/T_2$ as a function of (A) Dy (or Ho) and (B) combined Dy&Eu (or Ho&Eu or Ho&Tb) concentrations for aqueous sample solutions of D-glucuronic acid coated ultrasmall (I) $\text{Dy}_{1.5}\text{Eu}_{0.5}\text{O}_3$, (II) $\text{Ho}_{1.6}\text{Eu}_{0.4}\text{O}_3$, and (III) $\text{Ho}_{1.1}\text{Tb}_{0.9}\text{O}_3$ nanoparticles. (C) Plot of r_1 and r_2 values of three aqueous solutions estimated from single (“s”) and combined (“c”) concentration plots in (A) and (B), respectively. (D) R_1 and R_2 map images of three aqueous sample solutions (Ln = Dy in (I), and Ho in both (II) and (III)). (E) Plot of r_1 and r_2 values of various nanoparticles estimated at 1.5 tesla and 22°C: D-glucuronic coated Gd_2O_3 nanoparticle ($d_{\text{avg}} = 1.0 \text{ nm}$)⁵⁷, PEG-diacid coated Fe_3O_4 nanoparticle ($d_{\text{avg}} = 1.7 \text{ nm}$)⁵⁸, D-glucuronic acid coated MnO nanoparticle ($d_{\text{avg}} = 2.5 \text{ nm}$)⁵⁹, and three kinds of D-glucuronic acid coated ultrasmall mixed lanthanide oxide nanoparticles studied here.



were decent in all samples because of decent magnetizations of nanoparticles at room temperature. As expected, r_1 and r_2 values were comparable to those of unmixed lanthanide oxide nanoparticles^{25,53–56}. Both r_1 and r_2 values became reduced when they were estimated from combined concentration plots as shown in Fig. 5C. This simply come from concentration effect. r_2 values of combined concentration plots were reduced by $\sim 15 \text{ s}^{-1}\text{mM}^{-1}$ for $\text{Ln}_2 = \text{Tb}$ and $\sim 30 \text{ s}^{-1}\text{mM}^{-1}$ for $\text{Ln}_2 = \text{Eu}$ from the corresponding single concentration plots because Tb^{3+} has a slightly smaller magnetic moment than Ho^{3+} whereas Eu^{3+} , a lot smaller magnetic moment than both Dy^{3+} and Ho^{3+} (see Table 1).

As expected from negligible r_1 and decent r_2 values, negligible dose-dependent contrast enhancements in R_1 map images and appreciable dose-dependent contrast enhancements in R_2 map images were observed in all samples as shown in Fig. 5D. These results suggest that the present ultrasmall mixed lanthanide oxide nanoparticles are potential T_2 MRI contrast agents at high MR fields because their r_2 values and therefore their contrast enhancements in R_2 map images will further increase with MR field because r_2 is proportional to the square of MR field as mentioned before^{22–24}.

It will be valuable to compare r_1 and r_2 values of the present nanoparticles with those of other nanoparticles at similar particle diameters. As shown in Fig. 5E, gadolinium oxide nanoparticle showed the largest r_1 value because of a large electron spin magnetic moment ($S = 7/2$) of Gd^{3+} as mentioned before⁵⁷. Both Fe_3O_4 and MnO nanoparticles showed the next largest r_1 values because both Fe^{3+} and Mn^{2+} have $S = 5/2$ ^{58,59}. The present nanoparticles, however, showed negligible r_1 values because Dy^{3+} , Ho^{3+} , and Tb^{3+} have both electron orbital (L) and spin (S) magnetic moments as mentioned before, but the largest r_2 values due to their decent magnetic moments at room temperature. Therefore, as T_2 MRI contrast agents, the present nanoparticles are superior to other nanoparticles at ultrasmall particle diameters. This is important because ultrasmall nanoparticles are useful for in vivo applications because they can be excreted through renal system²⁷.

Fluorescent properties. Fluorescent properties of D-glucuronic acid coated ultrasmall mixed lanthanide oxide nanoparticles in ethanol were investigated by recording photoluminescent (PL) spectra as shown in Fig. 6. PL spectra of precursor ions in ethanol were also recorded as references as shown in Fig. 6. We observed constant emission intensities and identical PL spectra for repeated measurements, supporting good photostabilities of these nanoparticles.

As shown in Table 1 and Fig. 6, the main fluorescent lanthanide ions in sample solutions were Eu^{3+} and Tb^{3+} . The other ions negligibly contributed to PL spectra. Therefore, it was expected that PL spectra of sample solutions would resemble those of Eu^{3+} or Tb^{3+} precursor ions. However, PL spectra of sample solutions were quite different from those of these ions in two respects. First, PL spectra of sample solutions were generally broad. Second, new peaks (assigned as “*”) appeared with position and/or intensity quite different from those of precursor ions. These differences have been observed in various nano-systems such as polymer-based $\text{Eu}^{3+}/\text{Tb}^{3+}$ complex⁶⁰, $\text{Gd}_2\text{O}_3:\text{Eu}$ nanoparticles⁶¹, and $\text{Y}_2\text{O}_3:\text{Eu}$ nanoparticles⁶². Possibilities for these include the energy level coupling between emitting and other elements in nanoparticles⁶⁰, some disorder in nanoparticles (i.e., size effect)^{61,62}, and luminescence of surface elements in nanoparticles^{61,62}.

Fluorescent sample solutions in ethanol after irradiation with a mercury lamp are inserted at the top in Fig. 6. The fluorescent solution colours of ultrasmall $\text{Dy}_{1.5}\text{Eu}_{0.5}\text{O}_3$ and $\text{Ho}_{1.6}\text{Eu}_{0.4}\text{O}_3$ nanoparticles were slightly different from Eu^{3+} (red) due to their intense emissions at ~ 567 and ~ 562 nm, respectively, shorter than the main emission line of Eu^{3+} ($= 618$ nm). The fluorescent solution colour of ultrasmall $\text{Ho}_{1.1}\text{Tb}_{0.9}\text{O}_3$ nanoparticles was very different from Tb^{3+} (green) due to their intense emission at ~ 486 nm, much

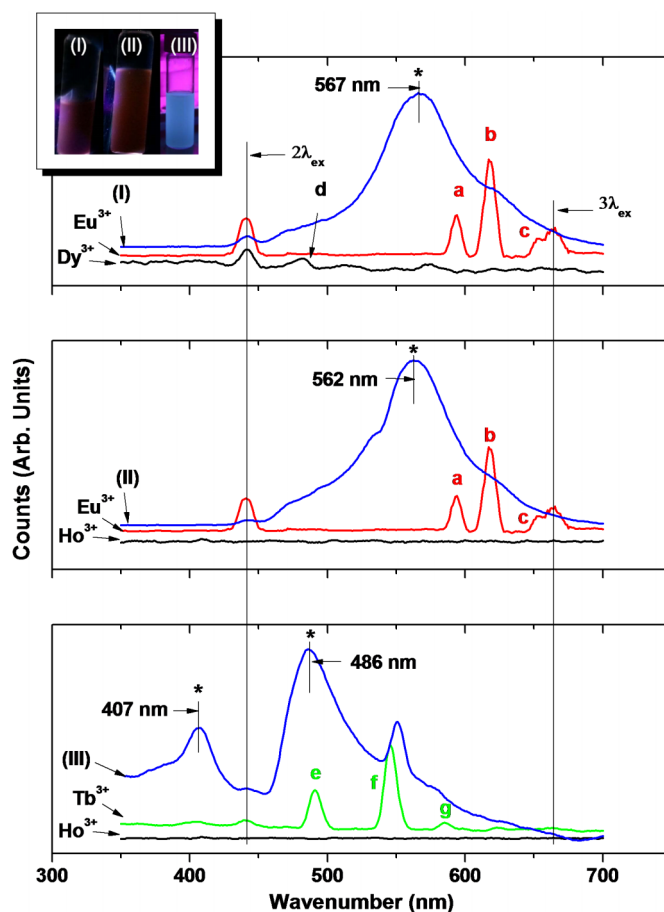


Figure 6 | PL spectra of sample solutions of D-glucuronic acid coated ultrasmall (I) $\text{Dy}_{1.5}\text{Eu}_{0.5}\text{O}_3$, (II) $\text{Ho}_{1.6}\text{Eu}_{0.4}\text{O}_3$, and (III) $\text{Ho}_{1.1}\text{Tb}_{0.9}\text{O}_3$ nanoparticles and four precursor ions ($\lambda_{\text{ex}} = 220$ nm, solvent = ethanol). The “*” indicates new peaks in nanoparticles with position and/or intensity quite different from those of precursor ions. Inserted at the top are photographs of the corresponding sample solutions after UV irradiation ($\lambda_{\text{ex}} = 254$ nm for samples (I) and (II), and 365 nm for sample (III), solvent = ethanol). The emission assignments in precursor ions are following: Eu^{3+} (a: ${}^5\text{D}_0 \rightarrow {}^7\text{F}_1$ (593 nm), b: ${}^5\text{D}_0 \rightarrow {}^7\text{F}_2$ (618 nm), c: ${}^5\text{D}_0 \rightarrow {}^7\text{F}_3$ (654 nm)); Dy^{3+} (d: ${}^4\text{F}_{9/2} \rightarrow {}^6\text{H}_{15/2}$ (480 nm)); Tb^{3+} (e: ${}^5\text{D}_4 \rightarrow {}^7\text{F}_6$ (491 nm), f: ${}^5\text{D}_4 \rightarrow {}^7\text{F}_5$ (545 nm), g: ${}^5\text{D}_4 \rightarrow {}^7\text{F}_4$ (584 nm)), which are consistent with reported values²⁸.

shorter than the main emission line of Tb^{3+} ($= 545$ nm). An emission colour different from those of precursor ions had been also observed in polymer-based $\text{Eu}^{3+}/\text{Tb}^{3+}$ complex⁶⁰ for the same reason, supporting our results.

Quantum yields (Φ s) of these nanoparticles in ethanol solution were estimated by using fluorescein as a standard ($\Phi = 0.95$)⁶³ at $\lambda_{\text{ex}} = 220$ nm. The Φ was 0.57 for ultrasmall $\text{Dy}_{1.5}\text{Eu}_{0.5}\text{O}_3$ nanoparticles, 0.43 for $\text{Ho}_{1.6}\text{Eu}_{0.4}\text{O}_3$ nanoparticles, and 0.48 for $\text{Ho}_{1.1}\text{Tb}_{0.9}\text{O}_3$ nanoparticles. These values are roughly consistent with those reported on lanthanide oxide nanoparticles by others^{64,65}, but slightly higher likely due to their ultrasmall particle diameters because it was found that fluorescent intensity of lanthanide oxide nanoparticles become enhanced with decreasing particle diameter^{15,16}.

In vitro cytotoxicity results. The toxicities of three aqueous sample solutions of D-glucuronic acid coated ultrasmall mixed lanthanide oxide nanoparticles were investigated by measuring cytotoxicity up to 400 (or 500) μM combined concentrations using both DU145 and NCTC1469 cells as shown in Fig. 7. They were non-toxic and thus, used for in vivo MR experiments.

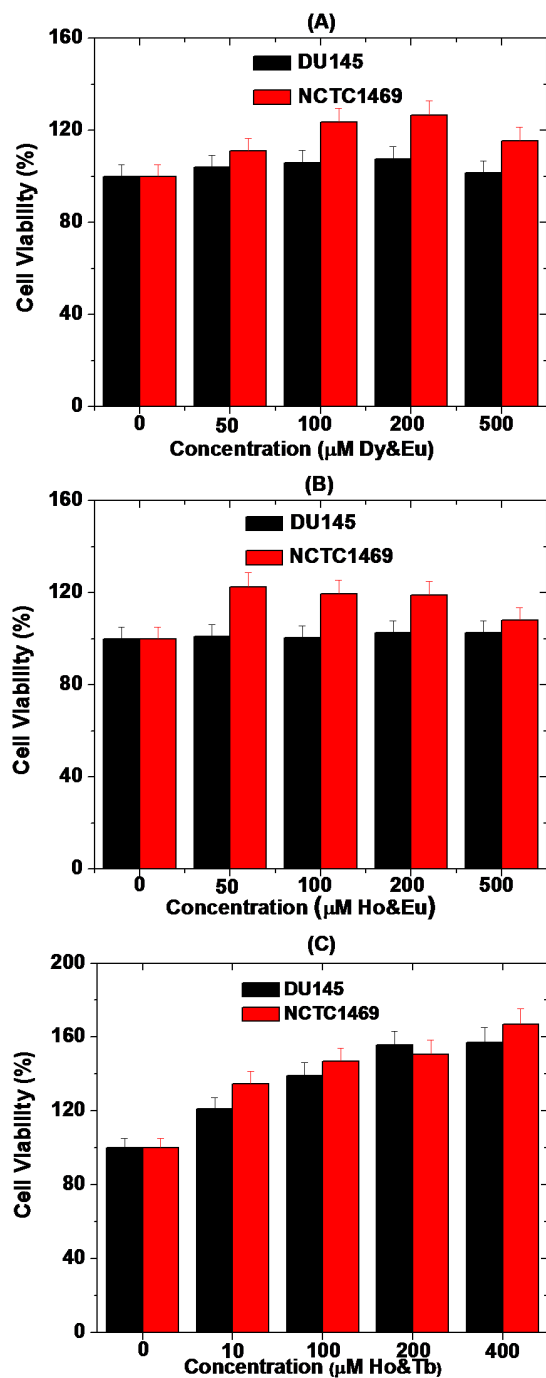


Figure 7 | In vitro cytotoxicity results of aqueous sample solutions of D-glucuronic acid coated ultrasmall (A) Dy_{1.5}Eu_{0.5}O₃, (B) Ho_{1.6}Eu_{0.4}O₃, and (C) Ho_{1.1}Tb_{0.9}O₃ nanoparticles using DU145 and NCTC1469 cells.

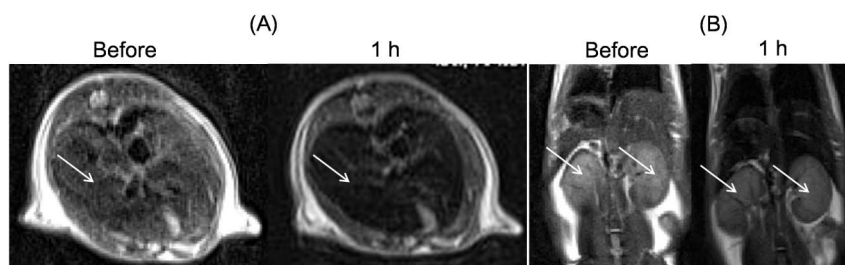


Figure 8 | 3 tesla T₂ MR images in a mouse: (A) axial views of liver and (B) coronal views of kidneys as indicated with arrows, respectively, before and one hour after injection of an aqueous sample solution of D-glucuronic acid coated ultrasmall Ho_{1.6}Eu_{0.4}O₃ nanoparticles into a mouse tail vein. MR images became darker after injection due to negative contrast enhancements by nanoparticles.

In vivo 3 tesla T₂ MR images. To measure in vivo 3 tesla T₂ MR images, aqueous sample solutions of D-glucuronic acid coated ultrasmall mixed lanthanide oxide nanoparticles were injected into a mouse tail vein. As shown in Fig. 8, decent negative contrast enhancements in both liver and kidneys were observed one hour after intravenous injection. Therefore, D-glucuronic acid coated ultrasmall mixed lanthanide oxide nanoparticles clearly functioned as T₂ MRI contrast agents. Stronger negative contrast enhancements will be observed at higher MR fields because r_2 is proportional to the square of applied MR field as mentioned before^{22–24}, implying that these nanoparticles are potential T₂ MRI contrast agents at high MR fields. Furthermore, antibodies, peptides or targeting molecules will increase the targeting ability of nanoparticles and as a result, provide the improved contrasts in MR images. More 3 tesla T₂ MR images in a mouse are provided in Supplementary data.

In vitro fluorescent confocal cellular images. To measure in vitro fluorescent confocal cellular images, aqueous sample solutions were treated to DU145 cells. Control DU145 cells to which no sample solution was treated were also prepared in the same condition. As shown at the top images in Figs. 9A to C, cell nuclei tinted pale blue at $\lambda_{ex} = 405$ nm because they were stained with 4',6 diamidino-2-phenylindole (DAPI). As shown at the bottom image in Fig. 9A, no fluorescence was observed in control cells at $\lambda_{ex} = 488$ nm. However, red fluorescence with treatment with Dy_{1.5}Eu_{0.5}O₃ nanoparticles (the bottom image in Fig. 9B) and green fluorescence with treatment with Ho_{1.1}Tb_{0.9}O₃ nanoparticles (the bottom image in Fig. 9C) were observed at $\lambda_{ex} = 488$ nm. These results demonstrated that ultrasmall mixed lanthanide oxide nanoparticles functioned sensitively as FI agents. More fluorescent confocal cellular images are provided in Supplementary data.

Discussion

In this study we demonstrated that ultrasmall mixed lanthanide oxide nanoparticles had excellent dual imaging properties. We used three systems of ultrasmall mixed lanthanide (Dy/Eu, Ho/Eu, and Ho/Tb) oxide nanoparticles to demonstrate this. The three main findings are following: (1) ultrasmall mixed lanthanide oxide nanoparticles are compact, robust, and stable, which is extremely useful for biomedical applications. They can be also easily synthesized with composition control. (2) They showed decent magnetizations at room temperature and as a result, appreciable r_2 values. Decent negative contrast enhancements in 3 tesla T₂ MR images in a mouse were observed, clearly demonstrating their capability as T₂ MRI contrast agents. Since r_2 is proportional to the square of MR field, these nanoparticles will be extremely useful as T₂ MRI contrast agents at high MR fields. (3) They strongly showed fluorescent confocal images in DU145 cells, clearly demonstrating their capability as FI agents. Therefore, ultrasmall mixed lanthanide oxide nanoparticles are potential dual T₂ MRI-FI agents that will be extremely useful for biomedical applications. It is worth to mention that although not studied here, we expect that ultrasmall mixed Dy/Tb

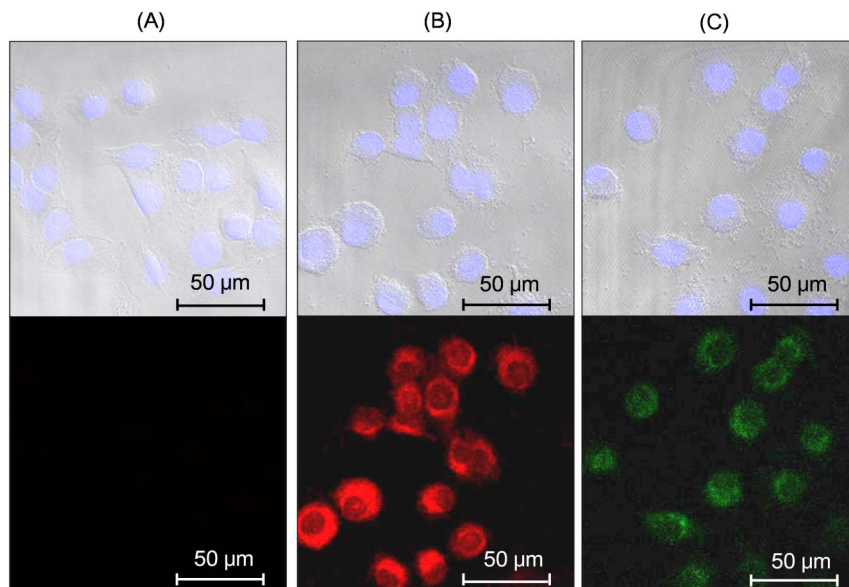


Figure 9 | Fluorescent confocal cellular images with $\lambda_{\text{ex}} = 405$ nm (top images) and 488 nm (bottom images): (A) the control DU145 cells and the DU145 cells treated with aqueous sample solutions of D-glucuronic acid coated ultrasmall (B) $\text{Dy}_{1.5}\text{Eu}_{0.5}\text{O}_3$ and (C) $\text{Ho}_{1.1}\text{Tb}_{0.9}\text{O}_3$ nanoparticles.

oxide nanoparticles will give similar results as those of the above three nano-systems studied in this work.

Mixed lanthanide oxide nanoparticles are extremely valuable for in vivo applications because they are compact, robust, and stable as mentioned above. This is critical because after intravenous injection they should not be decomposed and their properties should not be changed. As mentioned before, their magnetic properties do not much depend on surface coating and particle diameter due to compactness of 4f-orbitals close to nucleus¹⁴ and their fluorescent intensities rather enhance with decreasing particle diameter due to reduced excitation migration to quenching sites that are proportional to particle diameter^{15,16}, implying that they can be made ultrasmall without degrading their magnetic and fluorescent properties. Note that ultrasmall nanoparticles can be excreted through renal system²⁷, which is pre-requisite to in vivo applications. Therefore, ultrasmall mixed lanthanide oxide nanoparticles will be extremely useful for MRI-FI dual agents, as demonstrated in this study. For instance, a dual MRI-FI modality will allow us to detect and diagnose diseases very sensitively through FI and in a high spatial resolution through MRI.

In summary, we synthesized ultrasmall mixed lanthanide (Ln) oxide nanoparticles in which one Ln is used for MR imaging and the other Ln, for fluorescent imaging. We explored three systems (Dy/Eu, Ho/Eu, and Ho/Tb) in which Dy, Ho, and Tb are used for MR imaging and Eu and Tb, for fluorescent imaging. They clearly showed negative contrast in 3 tesla T_2 MR images in a mouse and a very intense fluorescence in confocal images in DU145 cells, demonstrating their usefulness as MRI-FI dual agents.

Methods

Chemicals. $\text{Dy}(\text{NO}_3)_3 \cdot x\text{H}_2\text{O}$ (99.9%), $\text{Ho}(\text{NO}_3)_3 \cdot 5\text{H}_2\text{O}$ (99.9%), $\text{Eu}(\text{NO}_3)_3 \cdot 5\text{H}_2\text{O}$ (99.9%), $\text{Tb}(\text{NO}_3)_3 \cdot 5\text{H}_2\text{O}$ (99.9%), NaOH (> 99.9%), 50% H_2O_2 aqueous solution, triethylene glycol (99%), CH_3OH (99.9%), and D-glucuronic acid (99.99%) were purchased from Sigma-Aldrich and used as received. $\text{C}_2\text{H}_5\text{OH}$ (99%) was purchased from Duksan (S. Korea) and used as received in washing nanoparticles. Triply distilled water was used for both washing nanoparticles and preparing sample solutions.

One-pot synthesis of D-glucuronic acid coated ultrasmall mixed Dy/Eu, Ho/Eu, and Ho/Tb oxide nanoparticles. 4 mmol of $\text{Dy}(\text{NO}_3)_3 \cdot x\text{H}_2\text{O}$ (or $\text{Ho}(\text{NO}_3)_3 \cdot 5\text{H}_2\text{O}$) and 1 mmol of $\text{Eu}(\text{NO}_3)_3 \cdot 5\text{H}_2\text{O}$ were added to 40 mL of triethylene glycol in a 100 mL three neck flask. The mixture solution was magnetically stirred at 40 °C under atmospheric condition until the precursor salts were completely dissolved in triethylene glycol. In a separate flask, NaOH solution was prepared by dissolving

15 mmol of NaOH in 5 mL of methanol. Then NaOH solution was slowly added to the above precursor solution using a syringe. The reaction temperature was raised to 240 °C and maintained at that temperature for 24 hours with magnetic stirring. The product nanoparticle solution was cooled to 80 °C for surface coating. In case of mixed Ho/Tb oxide nanoparticles, 2.5 mmol of $\text{Ho}(\text{NO}_3)_3 \cdot 5\text{H}_2\text{O}$ and 2.5 mmol of $\text{Tb}(\text{NO}_3)_3 \cdot 5\text{H}_2\text{O}$ were added to 40 mL of triethylene glycol. The mixture solution was magnetically stirred until the precursor salts were completely dissolved in triethylene glycol. The NaOH solution prepared in 5 mL of methanol in a separate flask was slowly added to the above precursor solution using a syringe. The mixture solution was magnetically stirred at 80 °C for 2 hours. Then 7.5 mL of 50% H_2O_2 aqueous solution was slowly added to the reaction solution using a syringe. After addition of H_2O_2 , the reaction mixture was magnetically stirred for additional 2 hours.

For surface coating, 5 mmol of D-glucuronic acid was added to the above nanoparticle solutions that were magnetically stirred at 80 °C for 24 hours under atmospheric condition. The product solutions were cooled to room temperature and transferred to 1 L beakers containing 500 mL of triply distilled water (or ethanol) to wash product nanoparticles. After nanoparticles settled to the beaker bottom, top transparent solutions were decanted and the remaining nanoparticles were washed again with triply distilled water (or ethanol) for three times. When ethanol was used as a washing solvent, nanoparticles were washed again with triply distilled water to remove ethanol. The first half volumes of washed nanoparticles were diluted with triply distilled water to prepare aqueous sample solutions and the remaining half volumes were reduced to powder form by drying them in air for various characterizations.

Characterizations. An ICPAES (Thermo Jarrell Ash Co., IRIS/AP) was used to measure the concentration of Ln (Ln = Dy, Ho, Eu, and Tb) in aqueous sample solutions. Ultrasmall particle diameters were estimated using a HRTEM (JEOL, JEM 2100F, 200 kV acceleration voltage) and a HVEM (JEOL JEM-ARM 1300 S, 1.2 MeV acceleration voltage). A copper grid (PELCO No.160, TED PELLA, INC.) covered with an amorphous carbon membrane was placed onto a filter paper and a nanoparticle solution diluted in triply distilled water or ethanol was dropped over the copper grid using a micropipette (Eppendorf, 2–20 μL). A DLS particle size analyzer (UPA-150, Microtrac) was used to measure the hydrodynamic diameters of D-glucuronic acid coated ultrasmall mixed lanthanide oxide nanoparticles dispersed in triply distilled water. The sample solution concentration used to measure hydrodynamic diameters was ~ 0.1 mM Ln (Ln = Dy, Ho, Eu or Tb). An XRD spectrometer (Philips, X'PERT PRO MRD) with an unfiltered $\text{CuK}\alpha$ radiation ($\lambda = 1.54184$ Å) was used to measure the crystal structure of powder samples of D-glucuronic acid coated ultrasmall mixed lanthanide oxide nanoparticles. The scanning step was 0.033° and scan range in 2θ was 15–100°. A FT-IR absorption spectrometer (Mattson Instruments, Inc., Galaxy 7020A) was used to investigate the surface coating in ultrasmall mixed lanthanide oxide nanoparticles. To record FT-IR absorption spectra (400–4000 cm^{-1}), pellets of powder samples in KBr were prepared. A TGA (TA Instruments, SDT-Q 600) was used to estimate the amount of surface coating with D-glucuronic acid in powder samples from the mass drop in TGA curves. TGA curves were recorded between room temperature and 900 °C while air flowed. A superconducting quantum interference device (SQUID) magnetometer (Quantum Design, MPMS-7) was used to measure the magnetic properties of ultrasmall mixed lanthanide oxide nanoparticles. Both M-H curves ($-5 \leq H \leq 5$



tesla) at $T = 5$ and 300 K and ZFC M-T curves ($5 \leq T \leq 300$ K) at $H = 0$ or 100 Oe were recorded. To measure both M-H and M-T curves, weighed powder samples were loaded into nonmagnetic gelatine capsules. To obtain net magnetizations of ultrasmall mixed lanthanide oxide nanoparticles in powder samples, observed magnetizations were mass-corrected using both powder sample masses and weight percents of ultrasmall mixed lanthanide oxide nanoparticles in powder samples estimated from TGA curves. A PL spectrometer (JASCO, FP-6500) was used to record PL spectra of D-glucuronic acid coated ultrasmall mixed lanthanide oxide nanoparticles dispersed in ethanol at $\lambda_{\text{ex}} = 220$ nm. The PL spectra of all precursor Ln^{3+} ($\text{Ln} = \text{Dy}, \text{Ho}, \text{Eu},$ and Tb) ions in ethanol were also recorded as references. Sample solution and precursor ion concentrations used to measure PL spectra were ~ 10 mM Ln ($\text{Ln} = \text{Eu}$ or Tb). Sample solutions were filled into a quartz cuvette with four optically clear sides (Sigma-Aldrich, 3 mL) for PL measurement. Quantum yields (Φ s) of sample solutions (1.0 mM in ethanol) were roughly estimated using fluorescein as a standard ($\Phi = 0.95$, 1.0 mM in 0.1 M NaOH ethanol solution)⁶³ at $\lambda_{\text{ex}} = 220$ nm. We used an equation of Φ (sample) $\approx \Phi$ (fluorescein) \times PL Intensity (sample)/PL Intensity (fluorescein) to estimate the Φ s of the sample solutions.

In vitro cytotoxicity measurement. A CellTiter-Glo Luminescent Cell Viability Assay (Promega, WI, USA) was used to measure the cellular toxicity of aqueous sample solutions of D-glucuronic acid coated ultrasmall mixed lanthanide oxide nanoparticles. In this assay, a luminometer (Victor 3, Perkin-Elmer) was used to quantify the intracellular adenosine triphosphate (ATP). Both human prostate cancer (DU145) and normal mouse hepatocyte (NCTC1469) cells were used as test cells. DMEM and RPMI1640 were used as culture media for NCTC1469 and DU145 cells, respectively. Cells were seeded on a 24-well cell culture plate and incubated for 24 hours (5×10^4 cell density, 500 μL cells per well, 5% CO_2 , and 37°C). Test sample solutions (10, 50, 100, 200, 400, 500 μM Ln_1 & Ln_2) ($\text{Ln}_1 = \text{Dy}$ or Ho , $\text{Ln}_2 = \text{Eu}$ or Tb) were prepared by diluting original sample solutions with a sterile phosphate-buffered saline (PBS) solution. Then, ~ 2 μL of each test sample solution was treated into the cultured cells, which were further incubated for 48 hours. Cell viability was measured and normalized with respect to the control cell with 0.0 M Ln concentration. The measurement was repeated twice for all sample cells to obtain average cell viabilities.

Relaxivity and map image measurement. A 1.5 tesla MRI instrument (GE 1.5 T Signa Advantage, GE medical system) equipped with the knee coil (EXTREM) was used to measure both T_1 and T_2 relaxation times as well as both R_1 and R_2 map images. A series of aqueous sample solutions with different concentrations (1, 0.5, 0.25, 0.125, 0.0625, and 0 mM Ln ($\text{Ln} = \text{Dy}$ or Ho)) were prepared by diluting original sample solutions with triply distilled water. Both relaxation times and map images were measured for these solutions. The r_1 and r_2 water proton relaxivities were then estimated from the slopes in the plots of $1/T_1$ and $1/T_2$ versus Ln ($\text{Ln} = \text{Dy}$ or Ho) or combined Ln_1 & Ln_2 ($\text{Ln}_1 = \text{Dy}$ or Ho , $\text{Ln}_2 = \text{Eu}$ or Tb) concentrations, respectively. The typical measurement parameters were as follows: the external MR field (H) = 1.5 tesla, the temperature (T) = 22°C , the number of acquisition (NEX) = 1, the field of view (FOV) = 16 cm, the phase FOV = 1 cm, the matrix size = 512×512 , the slice thickness = 5 mm, the spacing gap = 0 mm, the pixel bandwidth = 61.0547, the time of repetition (TR) = 2009 ms, and the time to echo (TE) = 9 ms.

In vivo 3 tesla T_2 MR image measurement. The animal experiments using mice in this study were approved by the animal research committee of Kyungpook National University (KNU) and carried out in accordance with its the rule. A 3 tesla MRI instrument (SIEMENS 3.0 T MAGNETOM Trio a Tim) was used to measure T_2 spin echo (SE) images of a mouse. An ICR female mouse with weight of ~ 30 g was used for each sample solution. Each mouse was anesthetized by 1.5% isoflurane in oxygen. Measurements were made before and after injection of a sample solution into a mouse tail vein. The injection dose was ~ 30 μL and ~ 0.05 mmol Ln_1 & Ln_2/kg ($\text{Ln}_1 = \text{Dy}$ or Ho , $\text{Ln}_2 = \text{Eu}$ or Tb). After measurement, a mouse was revived from anaesthesia and placed in a cage with a free access to both food and water. During measurement, each mouse was maintained at $\sim 37^\circ\text{C}$ by using a warm water blanket. The typical measurement parameters were as follows: (coronal view) $H = 3$ tesla, $T = 37^\circ\text{C}$, NEX = 3–4, FOV = 60 mm, the phase FOV = 60 mm, the matrix size = 256×256 , the slice thickness = 1 mm, the spacing gap = 0.1 mm, TR = 1620 ms, and TE = 37 ms; (axial view) $H = 3$ tesla, $T = 37^\circ\text{C}$, NEX = 3–4, FOV = 60 mm, the phase FOV = 30 mm, the matrix size = 128×256 , the slice thickness = 1 mm, the spacing gap = 0.1 mm, TR = 2690 ms, and TE = 37 ms.

In vitro fluorescent confocal cellular image measurement. A confocal laser scanning microscope (Carl Zeiss, LSM 700) equipped with a solid state laser was used to measure fluorescent images of DU145 cells. The DU145 cells were seeded onto two 35 mm cell culture dishes at the density of 2.5×10^5 per dish (2 mL, 5% CO_2 , 37°C). After 24 hours, one of the above two cell dishes was treated with ~ 50 μL of an aqueous sample solution (0.2–0.3 mM Eu or Tb) and incubated for 48 hours. The treated cells were washed with PBS solution twice. The untreated cells in the other dish served as control cells. The cells in both dishes were fixed with 4% paraformaldehyde (PFA) in PBS solution for 10 minutes at room temperature. After this, the cells in both dishes were washed again with PBS solution 3 times. The cell nuclei in both dishes were then stained with DAPI and washed again with PBS solution 3 times. The cells were mounted using Prolong Gold (Invitrogen, Carlsbad, CA, USA) for imaging. The laser power used for excitation was ~ 8 watts. The λ_{ex} s used for excitation of DAPI and nanoparticles were 405 and 488 nm, respectively. At

$\lambda_{\text{ex}} = 405$ nm, DAPI tinted pale blue. The typical magnifications used for imaging were 400 and 1000.

- Wang, G., Peng, Q. & Li, Y. Lanthanide-doped nanocrystals: synthesis, optical-magnetic properties, and applications. *Acc. Chem. Res.* **44**, 322–332 (2011).
- Xu, W. *et al.* T_1 , T_2 magnetic resonance imaging (MRI)-fluorescent imaging (FI) by using ultrasmall mixed gadolinium-europium oxide nanoparticles. *New J. Chem.* **36**, 2361–2367 (2012).
- Zhang, Y., Vijayaragavan, V., Das, G. K., Bhakoo, K. K. & Tan, T. T. Y. Single-phase $\text{NaDyF}_4:\text{Tb}^{3+}$ nanocrystals as multifunctional contrast agents in high-field magnetic resonance and optical imaging. *Eur. J. Inorg. Chem.* 2044–2048 (2012).
- Das, G. K. *et al.* Single-phase $\text{Dy}_2\text{O}_3:\text{Tb}^{3+}$ nanocrystals as dual-modal contrast agent for high field magnetic resonance and optical imaging. *Chem. Mater.* **23**, 2439–2446 (2011).
- Zhang, L. *et al.* Multifunctional $\text{GdPO}_4:\text{Eu}^{3+}$ hollow spheres: synthesis and magnetic and luminescent properties. *Inorg. Chem.* **50**, 10608–10613 (2011).
- Tian, G. *et al.* Facile fabrication of rare-earth doped Gd_2O_3 hollow spheres with upconversion luminescence, magnetic resonance, and drug delivery properties. *J. Phys. Chem. C* **115**, 23790–23796 (2011).
- Li, I.-F. & Yeh, C.-S. Synthesis of Gd doped CdSe nanoparticles for potential optical and MR imaging applications. *J. Mater. Chem.* **20**, 2079–2081 (2010).
- Zhou, J. *et al.* Dual-modality in vivo imaging using rare-earth nanocrystals with near-infrared to near-infrared (NIR-to-NIR) upconversion luminescence and magnetic resonance properties. *Biomaterials* **31**, 3287–3295 (2010).
- Shi, Z., Neoh, K. G., Kang, E. T., Shuter, B. & Wang, S.-C. Bifunctional Eu^{3+} -doped Gd_2O_3 nanoparticles as a luminescent and T_1 contrast agent for stem cell labeling. *Contrast Media Mol. Imaging* **5**, 105–111 (2010).
- Petral, Jr, R. M. *et al.* Synthesis and characterization of Tb^{3+} -doped Gd_2O_3 nanocrystals: a bifunctional material with combined fluorescent labeling and MRI contrast agent properties. *J. Phys. Chem. C* **113**, 6913–6920 (2009).
- Kim, H., Achermann, M., Balet, L. P., Hollingsworth, J. A. & Klimov, V. I. Synthesis and characterization of Co/CdSe core/shell nanocomposites: bifunctional magnetic-optical nanocrystals. *J. Am. Chem. Soc.* **127**, 544–546 (2005).
- Gu, H. W., Zheng, R. K., Zhang, X. X. & Xu, B. Facile one-pot synthesis of bifunctional heterodimers of nanoparticles: a conjugate of quantum dot and magnetic nanoparticles. *J. Am. Chem. Soc.* **126**, 5664–5665 (2004).
- Xu, W. *et al.* Fluorescein-polyethyleneimine coated gadolinium oxide nanoparticles as T_1 magnetic resonance imaging (MRI)-cell labeling (CL) dual agents. *RSC Adv.* **2**, 10907–10915 (2012).
- Cotton, F. A. & Wilkinson, G. *Advanced Inorganic Chemistry*, 4th Edn. [983] (John Wiley & Sons, New York, 1980).
- Wakefield, G., Keron, H. A., Dobson, P. J. & Hutchison, J. L. Synthesis and properties of sub-50-nm europium oxide nanoparticles. *J. Colloid Interface Sci.* **215**, 179–182 (1999).
- Flores-González, M. A. *et al.* Elaboration of nanostructured Eu^{3+} -doped Gd_2O_3 phosphor fine spherical powders using polyol-mediated synthesis. *Appl. Phys. A - Mater. Sci. Proc.* **81**, 1385–1391 (2005).
- Lewin, M. *et al.* Tat peptide-derivatized magnetic nanoparticles allow in vivo tracking and recovery of progenitor cells. *Nat. Biotechnol.* **18**, 410–414 (2000).
- Lux, F. *et al.* Ultrasmall rigid particles as multimodal probes for medical applications. *Angew. Chem. Int. Ed.* **50**, 12299–12303 (2011).
- Weissleder, R. & Mahmood, U. Molecular imaging. *Radiology* **219**, 316–333 (2001).
- Paeng, J. C. & Lee, D. S. Multimodal molecular imaging in vivo. *Open Nucl. Med. J.* **2**, 145–152 (2010).
- Kircher, M. F., Mahmood, U., King, R. S., Weissleder, R. & Josephson, L. A multimodal nanoparticle for preoperative magnetic resonance imaging and intraoperative optical brain tumor delineation. *Cancer Res.* **63**, 8122–8125 (2003).
- Lauffer, R. B. Paramagnetic metal complexes as water proton relaxation agents for NMR imaging: theory and design. *Chem. Rev.* **87**, 901–927 (1987).
- Caravan, P., Ellison, J. J., McMurry, T. J. & Lauffer, R. B. Gadolinium(III) chelates as MRI contrast agents: structure, dynamics, and applications. *Chem. Rev.* **99**, 2293–2352 (1999).
- Roch, A., Muller, R. N. & Gillis, P. Theory of proton relaxation induced by superparamagnetic particles. *J. Chem. Phys.* **110**, 5403–5411 (1999).
- Kattel, K. *et al.* A facile synthesis, in vitro and in vivo MR studies of D-glucuronic acid-coated ultrasmall Ln_2O_3 ($\text{Ln} = \text{Eu}, \text{Gd}, \text{Dy}, \text{Ho},$ and Er) nanoparticles as a new potential MRI contrast agent. *ACS Appl. Mater. Interfaces* **3**, 3325–3334 (2011).
- Xu, W. *et al.* Paramagnetic nanoparticle T_1 and T_2 MRI contrast agents. *Phys. Chem. Chem. Phys.* **14**, 12687–12700 (2012).
- Choi, H. S. *et al.* Renal clearance of quantum dots. *Nat. Biotechnol.* **25**, 1165–1170 (2007).
- Bünzli, J.-C. G. Lanthanide luminescence for biomedical analyses and imaging. *Chem. Rev.* **110**, 2729–2755 (2010).
- Eliseeva, S. V. & Bünzli, J.-C. G. Lanthanide luminescence for functional materials and bio-sciences. *Chem. Soc. Rev.* **39**, 189–227 (2010).
- Michalet, X. *et al.* Quantum dots for live cells, in vivo imaging, and diagnostics. *Science* **307**, 538–544 (2005).



31. Lin, S. *et al.* Quantum dot imaging for embryonic stem cells. *BMC Biotechnol.* **7**, 67 (2007).
32. Kovar, J. L., Simpson, M. A., Schutz - Geschwender, A. & Olive, D. M. A systematic approach to the development of fluorescent contrast agents for optical imaging of mouse cancer models. *Anal. Biochem.* **367**, 1–12 (2007).
33. Wu, S. *et al.* Non-blinking and photostable upconverted luminescence from single lanthanide-doped nanocrystals. *Proc. Natl. Acad. Sci. USA* **106**, 10917–10921 (2009).
34. Lim, S. F. *et al.* In vivo and scanning electron microscopy imaging of upconverting nanophosphors in *Caenorhabditis elegans*. *Nano Lett.* **6**, 169–174 (2006).
35. Chatterjee, D. K., Rufaihah, A. J. & Zhang, Y. Upconversion fluorescence imaging of cells and small animals using lanthanide doped nanocrystals. *Biomaterials* **29**, 937–943 (2008).
36. Sun, S., Murray, C. B., Weller, D., Folks, L. & Moser, A. Monodisperse FePt nanoparticles and ferromagnetic FePt nanocrystal superlattices. *Science* **287**, 1989–1992 (2000).
37. Park, J. *et al.* Ultra-large-scale syntheses of monodisperse nanocrystals. *Nat. Mater.* **3**, 891–895 (2004).
38. Wang, F. *et al.* Simultaneous phase and size control of upconversion nanocrystals through lanthanide doping. *Nat.* **463**, 1061–1065 (2010).
39. Söderlind, F., Pedersen, H., Petoral Jr, R. M., Käll, P.-O. & Uvdal, K. Synthesis and characterization of Gd₂O₃ nanocrystals functionalized by organic acids. *J. Colloid Interface Sci.* **288**, 140–148 (2005).
40. Duckworth, O. W. & Martin, S. T. Surface complexation and dissolution of hematite by C₁–C₆ dicarboxylic acids at pH = 5.0. *Geochim. Cosmochim. Acta* **65**, 4289–4301 (2001).
41. Hug, S. J. & Bahnemann, D. Infrared spectra of oxalate, malonate and succinate adsorbed on the aqueous surface of rutile, anatase and lepidocrocite measured with in situ ATR-FTIR. *J. Electron Spectrosc. Relat. Phenom.* **150**, 208–219 (2006).
42. Hug, S. J. & Sulzberger, B. In situ Fourier transform infrared spectroscopic evidence for the formation of several different surface complexes of oxalate on TiO₂ in the aqueous phase. *Langmuir* **10**, 3587–3597 (1994).
43. Mendive, C. B., Bredow, T., Blesa, M. A. & Bahnemann, D. W. ATR-FTIR measurements and quantum chemical calculations concerning the adsorption and photoreaction of oxalic acid on TiO₂. *Phys. Chem. Chem. Phys.* **8**, 3232–3247 (2006).
44. Corbierre, M. K., Cameron, N. S. & Lennox, R. B. Polymer-stabilized gold nanoparticles with high grafting densities. *Langmuir* **20**, 2867–2873 (2004).
45. Aaraj, S. & Colvin, R. V. Paramagnetic susceptibility of Eu₂O₃ from 300° to 1300°K. *J. Appl. Phys.* **35**, 1181–1183 (1964).
46. Aaraj, S. & Colvin, R. V. Magnetic susceptibility of gadolinium and dysprosium sesquioxides at elevated temperatures. *J. Appl. Phys.* **33**, 2517–2519 (1962).
47. Koehler, W. C., Wollan, E. O. & Wilkinson, M. K. Paramagnetic and nuclear scattering cross sections of holmium sesquioxide. *Phys. Rev.* **110**, 37–40 (1958).
48. Lal, H. B., Pratap, V. & Kumar, A. Magnetic susceptibility of heavy rare-earth sesquioxides. *Pramāna* **10**, 409–412 (1978).
49. Bridot, J.-L. *et al.* Hybrid gadolinium oxide nanoparticles: multimodal contrast agents for in vivo imaging. *J. Am. Chem. Soc.* **129**, 5076–5084 (2007).
50. Ahrén, M. *et al.* Synthesis and characterization of PEGylated Gd₂O₃ nanoparticles for MRI contrast enhancement. *Langmuir* **26**, 5753–5762 (2010).
51. Johnson, N. J. J., Oakden, W., Stanis, G. J., Prosser, R. S. & van Veggel, F. C. J. M. Size-tunable, ultrasmall NaGdF₄ nanoparticles: insight into their T₁ MRI contrast enhancement. *Chem. Mater.* **23**, 3714–3722 (2011).
52. Kim, T. J., Chae, K. S., Chang, Y. & Lee, G. H. Gadolinium oxide nanoparticles as potential multimodal imaging and therapeutic agents. *Curr. Topics Med. Chem.* **13**, 422–433 (2013).
53. Kattel, K. *et al.* Paramagnetic dysprosium oxide nanoparticles and dysprosium hydroxide nanorods as T₂ MRI contrast agents. *Biomaterials* **33**, 3254–3261 (2012).
54. Norek, M., Kampert, E., Zeitler, U. & Peters, J. A. Tuning of the size of Dy₂O₃ nanoparticles for optimal performance as an MRI contrast agent. *J. Am. Chem. Soc.* **130**, 5335–5340 (2008).
55. Norek, M. *et al.* NMR transversal relaxivity of suspensions of lanthanide oxide nanoparticles. *J. Phys. Chem. C* **111**, 10240–10246 (2007).
56. Gossuin, Y. *et al.* Physico-chemical and NMR relaxometric characterization of gadolinium hydroxide and dysprosium oxide nanoparticles. *Nanotechnology* **19**, 475102 (2008).
57. Park, J. Y. *et al.* Paramagnetic ultrasmall gadolinium oxide nanoparticles as advanced T₁ MRI contrast agent: account for large longitudinal relaxivity, optimal particle diameter, and in vivo T₁ MR images. *ACS Nano* **3**, 3663–3669 (2009).
58. Park, J. Y., Daksha, P., Lee, G. H., Woo, S. & Chang, Y. Highly water-dispersible PEG surface modified ultra small superparamagnetic iron oxide nanoparticles useful for target-specific biomedical applications. *Nanotechnology* **19**, 365603 (2008).
59. Baek, M. J. *et al.* Water-soluble MnO nanocolloids for a molecular T₁ MR imaging: a facile one-pot synthesis, in vivo T₁ MR images, and account for relaxivities. *ACS Appl. Mater. Interfaces* **2**, 2949–2955 (2010).
60. Shunmugam, R. & Tew, G. N. Unique emission from polymer based lanthanide alloys. *J. Am. Chem. Soc.* **127**, 13567–13572 (2005).
61. Bazzi, R. *et al.* Synthesis and properties of europium-based phosphors on the nanometer scale: Eu₂O₃, Gd₂O₃:Eu, and Y₂O₃:Eu. *J. Colloid Interface Sci.* **273**, 191–197 (2004).
62. Zhang, W.-W. *et al.* Optical properties of nanocrystalline Y₂O₃:Eu depending on its odd structure. *J. Colloid Interface Sci.* **262**, 588–593 (2003).
63. Brouwer, A. M. Standards for photoluminescence quantum yield measurements in solution (IUPAC Technical Report). *Pure Appl. Chem.* **83**, 2213–2228 (2011).
64. Hasegawa, Y. *et al.* Enhanced luminescence and photomagnetic properties of surface-modified EuO nanocrystals. *Angew. Chem. Int. Ed.* **41**, 2073–2075 (2002).
65. Stouwdam, J. W., Hebbink, G. A., Huskens, J. & van Veggel, F. C. J. M. Lanthanide-doped nanoparticles with excellent luminescent properties in organic media. *Chem. Mater.* **15**, 4604–4616 (2003).

Acknowledgments

This study was supported by the Basic Science Research Program through the National Research Foundation funded by the Ministry of Education, Science, and Technology (Grant No. 2012R1A1B3004241 to K.S.C., 2011-0015353 to Y.C., 2013R1A1A4A03004511 to G.H.L., and 2010-0024143 to T.J.K.) and the Basic Research Laboratory (BRL) Program (2013), the R&D program of MKE/KEIT (Grant No. 10040393, development and commercialization of molecular diagnostic technologies for lung cancer through clinical validation), and the KNU Research Fund (2013). We thank the Korea Basic Science Institute for the use of their HRTEM, HVEM, and XRD.

Author contributions

W.X., B.A.B. and C.R.K. carried out syntheses and characterizations of nanoparticles, J.S.B. and Y.C. measured relaxivities and T₂ MR images, J.E.B. and K.S.C. measured cytotoxicities and fluorescent confocal images, and Y.C., T.J.K. and G.H.L. led the project.

Additional information

Supplementary information accompanies this paper at <http://www.nature.com/scientificreports>

Competing financial interests: The authors declare no competing financial interests.

How to cite this article: Xu, W.L. *et al.* Mixed lanthanide oxide nanoparticles as dual imaging agent in biomedicine. *Sci. Rep.* **3**, 3210; DOI:10.1038/srep03210 (2013).



This work is licensed under a Creative Commons Attribution-NonCommercial-NoDerivs 3.0 Unported license. To view a copy of this license, visit <http://creativecommons.org/licenses/by-nc-nd/3.0>